Theor Appl Climatol (2018) 133:1107–1118
DOI 10.1007/s00704-017-2240-4

ORIGINAL PAPER

Multi-model ensemble projections of future extreme heat stress on rice across southern China

Liang He[1] · James Cleverly[2] · Bin Wang[3] · Ning Jin[4] · Chunrong Mi[5] · De Li Liu[3] · Qiang Yu[2,4,6]

Received: 18 March 2017 / Accepted: 31 July 2017 / Published online: 17 August 2017

Abstract Extreme heat events have become more frequent and intense with climate warming, and these heatwaves are a threat to rice production in southern China. Projected changes in heat stress in rice provide an assessment of the potential impact on crop production and can direct measures for adaptation to climate change. In this study, we calculated heat stress indices using statistical scaling techniques, which can efficiently downscale output from general circulation models (GCMs). Data across the rice belt in southern China were obtained from 28 GCMs in the Coupled Model Intercomparison Project phase 5 (CMIP5) with two emissions scenarios (RCP4.5 for current emissions and RCP8.5 for increasing emissions). Multi-model ensemble projections over the historical period (1960–2010) reproduced the trend of observations in heat stress indices (root-mean-square error RMSE = 6.5 days) better than multi-model arithmetic mean (RMSE 8.9 days) and any individual GCM (RMSE 11.4 days). The frequency of heat stress events was projected to increase by 2061–2100 in both scenarios (up to 185 and 319% for RCP4.5 and RCP8.5, respectively), especially in the middle and lower reaches of the Yangtze River. This increasing risk of exposure to heat stress above 30 °C during flowering and grain filling is predicted to impact rice production. The results of our study suggest the importance of specific adaption or mitigation strategies, such as selection of heat-tolerant cultivars and adjustment of planting date in a warmer future world.

1 Introduction

Climate change is characterized by increasing temperature, modified precipitation patterns, and increasing frequency of extreme weather events. Global average temperature has increased by 0.85 °C between 1880 and 2012 (IPCC 2013). In the last 50 years, temperatures have increased by 0.15–0.40 °C per decade in China (Piao et al. 2010). Not only is temperature increasing, extreme climate events such as heatwaves will become more frequent in the future (Shen et al. 2016; Sun et al. 2014). These changes in global climate can detrimentally affect crop phenology (Tao et al. 2014; Zhang et al., 2013), production, and water use (Shuai et al., 2014; Tao and Zhang 2013; Yao et al. 2007).

Rice is one of the most important staple foods globally, feeding more than half of the world's population. Rice provides a livelihood for farmers in Asia, Latin America, and increasingly in Africa (Jagadish et al. 2014). China is the largest producer of rice, accounting for 18.5% of the world's rice planting area and 28% of the world's rice production (Shi et al. 2015a, b). As rice is usually planted in subtropical regions, exposure to acute high temperature is a common risk. Heat stress can cause a dramatic reduction in yield, particularly during reproductive periods (Jagadish et al. 2007). For

✉ Liang He
heliang@cma.gov.cn; heliang_hello@163.com

1 National Meteorological Center, Beijing 100081, China

2 School of Life Sciences, University of Technology Sydney, PO Box 123, Broadway, Sydney, NSW 2007, Australia

3 NSW Department of Primary Industries, Wagga Wagga Agricultural Institute, Wagga Wagga, NSW 2650, Australia

4 State Key Laboratory of Soil Erosion and Dryland Farming on the Loess Plateau, Northwest A&F University, Yangling 712100, China

5 Key Laboratory of Water Cycle and Related Land Surface Processes, Institute of Geographic Sciences and Natural Resources Research, Beijing 100101, China

6 College of Resources and Environment, University of Chinese Academy of Science, Beijing 100049, China

example, rice yield in China decreased by 1.5–9.7% due to heat stress in the past three decades (Shi et al. 2015a; Zhang et al. 2016). Rice yield decreased by 10% in the Philippines due to a 1 °C increase in minimum temperature (Peng et al. 2004). Simulation results in the rice belt of China (Yao et al. 2007) indicated that variation of rice yields would increase due to climate change. Heat stress has become one of the worst threats for rice production in a warmer future (Jagadish et al. 2014; Sánchez et al., 2014; Wang et al. 2014b).

Previous research into the influence of heat stress on rice production mainly focused on historical effects of heat stress (Huang et al. 2016; Shi et al. 2015a; Sun and Huang 2011; Zhang et al., 2016), mechanisms of heat stress damage (Jagadish et al. 2007), or modeling (Shi et al. 2015a, b). For example, historical data indicate that heat stress increased from 1981 to 2010 in most areas of southern China (Shi et al. 2015a). Jagadish et al. (2007) studied the effects of duration of exposure to high temperature on spikelet fertility and found less than 1 h of exposure to high temperature is sufficient to induce sterility in rice. Shi et al. (2015b) found further effects of extreme high temperature on rice phenology. However, what extent of rice heat stress in the future scenarios is less known. Additionally, future heat stress risk is also uncertain due to uncertainty of different GCMs and multi-model ensemble methods. Consequently, it is essential to quantify what extents of exposure to heat stress for rice in the future, which can be done using ensemble results of general circulation models (GCMs).

GCMs have projected extreme temperatures in the future (Jiang et al. 2012; Sillmann and Roeckner, 2008). However, output data from GCMs cannot be directly used in the site-specific impacts of climate change on crops due to the coarse spatial and temporal resolution of GCMs. Downscaling methods can obtain high-resolution or site-specific climate data, either by dynamical downscaling or by statistical downscaling (Vaittinada Ayar et al. 2016). Dynamical downscaling has a high computational cost due to nesting of regional climate models (Liu and Zuo 2012). Statistical downscaling has a low computational cost for obtaining site-specific data under different emissions scenarios. This method usually applies statistical transfer functions, stochastic weather generators, or weather typing based on GCM outputs (Vaittinada Ayar et al. 2016). In this study, we used the statistical downscaling method proposed by Liu and Zuo (2012), which uses a stochastic weather generator to obtain daily and site-specific data from multiple GCMs under various future emissions scenarios, including RCP4.5 and RCP8.5.

The role of heat stress on rice in the future is less well known due to uncertainty in various GCMs. There is not a GCM that can be considered as the best model due to the complexity of the climate system (Knutti and Sedlacek 2013; Tebaldi and Knutti 2007). To reduce uncertainty, multi-model ensembles combine results from multiple models using weighting approaches such as Bayesian methods (Tebaldi et al. 2005). Bishop and Abramowitz (2013) developed a new strategy called the independence-weighted mean (IWM) that accounted for inter-model dependence and was defined using covariances of model errors. IWM estimates are weighted as a linear combination of model simulations in the ensemble. In this study, we used IWM to estimate heat stress indices specific to rice.

We firstly analyzed heat stress indices for rice in the southern China by statistically down-scaling the data from 28 GCMs. We next applied the IWM approach to ensemble heat stress indices from outputs of the GCMs. We hypothesized that the frequency and intensity of heatwaves would increase in the future, potentially affecting yield and survival in rice of southern China.

2 Materials and methods

2.1 Study region and observed meteorological sites

Rice production in China is mainly distributed to the South, including 18 provinces, autonomous regions, or municipalities (Fig. 1). Rice accounts for 84% of planting area in this region and 83% of the total rice production in China. The planting area for rice across this region was 25,412,000 ha per year on average (for the period 2010–2014), ranging from 4,079,500 ha per year in Hunan province to 104,000 ha per year in Shanghai. Two seasons of rice production per year occur in the South, mainly distributed in Hunan, Jiangxi, Zhejiang, Fujian, Guangdong, Guangxi, and the south of Anhui. To the North of this double-season rice belt, a single crop is obtained each year (Fig. 1).

The China Meteorological Administration (CMA) provides data from up to 170 meteorological stations from 1960 to 2010. These historical data include maximum and minimum temperature, precipitation, wind speed, relative humidity, etc. Temperature data were used to calculate observed heat stress indices over the historical period (1960–2010) and for statistical downscaling.

2.2 Rice heat stress indices

Short-term exposure to heat above 33 °C during anthesis in rice can lead to sterility, whereas exposure to temperatures below 29.6 °C during this crucial stage does not (Jagadish et al. 2007). Heat stress indices were thus chosen to reflect the risk to growth, survival, and yield in rice following national standards (GB/T 21985, 2008) and previous studies (Tao and Zhang 2013; Zhang et al. 2014). These heat stress indices are listed in Table 1. Heat stress was evaluated relative to daily mean (30 °C) or maximum temperature (35 °C) and all days versus during heatwaves of 3 days or more in length.

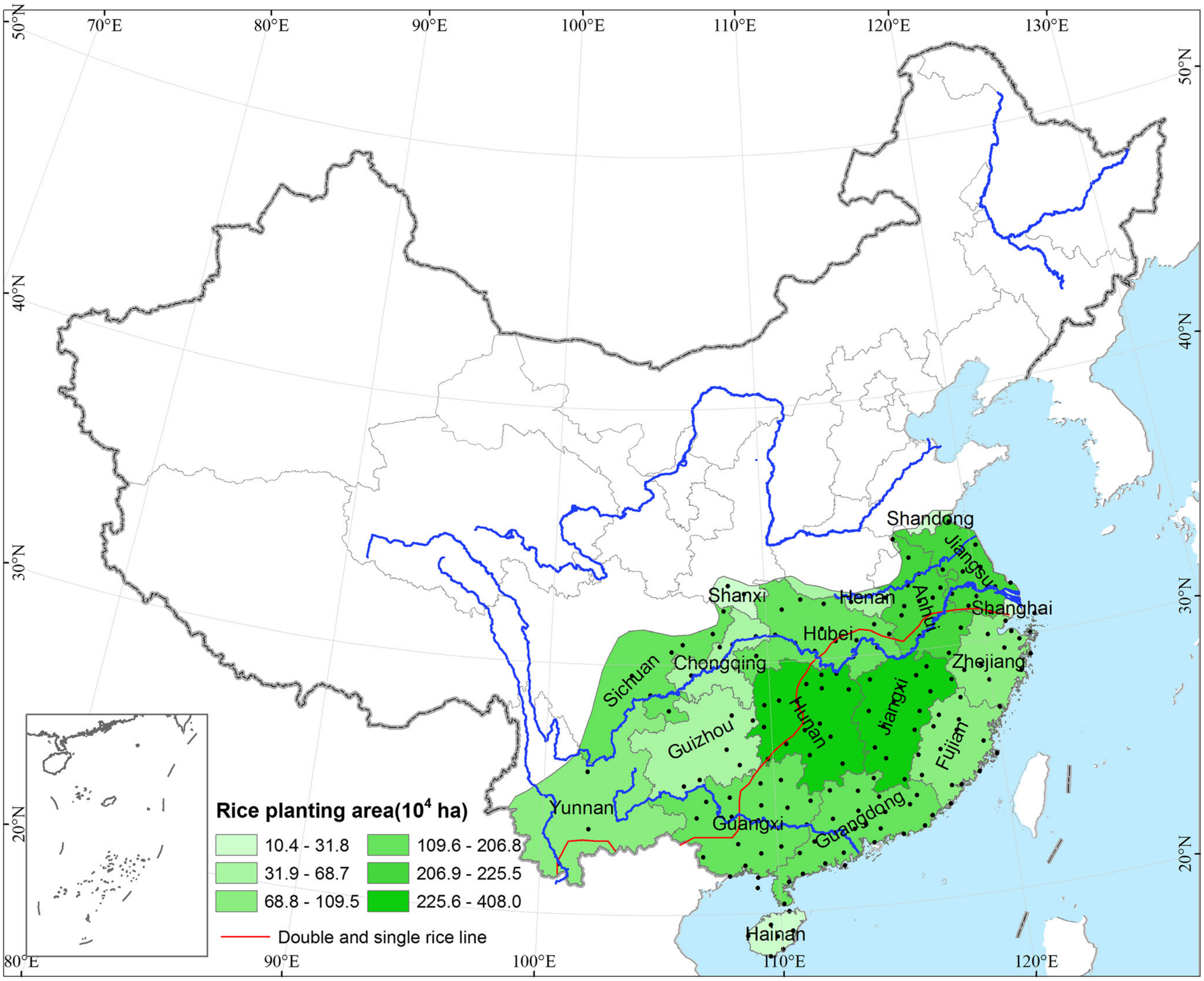

Fig. 1 Rice planting area in southern China and observed meteorological sites in this study. The panel in the figure is South China Sea Islands

Heat stress usually occurs during several stages: booting, heading, flowering, and milky ripening. Booting, heading, and flowering are the most sensitive stages associated with reduced crop yield due to heat stress. Because of differing phenology across the rice belt, we calculated the heat stress indices during the period from June 1 to August 31. Booting, heading, and flowering in rice usually occur during this period. Furthermore, heat stress also occurs more frequently during this period.

2.3 GCMs, statistical downscaling method, and climate projections

The data of 28 GCMs were obtained from the Coupled Model Inter-comparison Project phase 5 (CMIP5; Table 2). The detailed description of CMIP5 can be found at the website http://cmip-pcmdi.llnl.gov/cmip5/docs/CMIP5_modeling_groups.pdf. These 28 GCMs were selected because no single model can capture the complexity of the climate system.

Table 1 Definitions of heat stress indices used in this study

Abbr. of index	Definition	Unit
MeanT30days	The number of days with daily average temperature ≥ 30 °C temperature °C	days
MeanT30daysMore3	The number of days with three or more continuous days of daily average temperature ≥ 30°C with daily average temperature ≥ 30 °C	days
MaxT35days	The number of days with daily maximum temperature ≥ 35 °C	days
MaxT35daysMore3	The number of days with three or more continuous days of daily maximum temperature ≥ 35 °C	days

Table 2 28 GCMs used in this study for statistical downscaled outputs of 170 sites (Liu and Zuo 2012)

Model no.	Name of GCM	Abbr. of GCM	Institute ID	Country
01	BCC-CSM1.1	BC1	BCC	China
02	BCC-CSM1.1(m)	BC2	BCC	China
03	BNU-ESM	BNU	GCESS	China
04	CanESM2	CaE	CCCMA	Canada
05	CCSM4	CCS	NCAR	USA
06	CESM1(BGC)	CE1	NSF-DOE-NCAR	USA
07	CMCC-CM	CM2	CMCC	Europe
08	CMCC-CMS	CM3	CMCC	Europe
09	CSIRO-Mk3.6.0	CSI	CSIRO-QCCCE	Australia
10	EC-EARTH	ECE	EC-EARTH	Europe
11	FIO-ESM	FIO	FIO	China
12	GISS-E2-H-CC	GE2	NASA GISS	USA
13	GISS-E2-R	GE3	NASA GISS	USA
14	GFDL-CM3	GF2	NOAA GFDL	USA
15	GFDL-ESM2G	GF3	NOAA GFDL	USA
16	GFDL-ESM2M	GF4	NOAA GFDL	USA
17	HadGEM2-AO	Ha5	NIMR/KMA	Korea
18	INM-CM4	INC	INM	Russia
19	IPSL-CM5A-MR	IP2	IPSL	France
20	IPSL-CM5B-LR	IP3	IPSL	France
21	MIROC5	MI2	MIROC	Japan
22	MIROC-ESM	MI3	MIROC	Japan
23	MIROC-ESM-CHEM	MI4	MIROC	Japan
24	MPI-ESM-LR	MP1	MPI-M	Germany
25	MPI-ESM-MR	MP2	MPI-M	Germany
26	MRI-CGCM3	MR3	MRI	Japan
27	NorESM1-M	NE1	NCC	Norway
28	NorESM1-ME	NE2	NCC	Norway

We used the statistical downscaling method developed by Liu and Zuo (2012), which is rapid and reliable, and it is capable of stochastically generating daily climate series from monthly projections based on a modified version of the WGEN weather generator (Richardson and Wright 1984). The statistical downscaling method relies on empirical relationships between observational data and data from GCM simulations. There are usually two procedures, separately performing spatial and temporal downscaling. Firstly, monthly GCM simulations were downscaled to specific sites (in this case 170 sites in the rice belt of southern China, Fig. 1) using the inverse distance-weighted (IDW) interpolation method. A bias correction procedure was used during this step to correct site-based monthly GCM values. Secondly, daily climate variables (maximum and minimum temperature and precipitation) were temporally scaled for each site from the spatially downscaled projections by using the WGEN stochastic weather generator. Unlike other statistical downscaling methods, this method does not require atmospheric circulation or sea surface temperature as predictors. In addition, it can easily obtain daily climate series on a small computer, thus minimizing computational time and cost relative to dynamic downscaling. This simplified approach is effective at generating daily climate sequences for studies of future climate extremes (Wang et al. 2016) and climate impacts on crops (Anwar et al. 2015; Yang et al. 2014).

Liu and Zuo (2012) tested the improved WGEN procedure by which daily climate was generated from monthly observations. In our study, the performance of the statistical downscaling model was evaluated through comparisons between the distributions of measured and downscaled climate data using the Kruskall-Wallis rank (K-W) and Siegel-Tukey rank sum dispersion (S-T) tests. As the following describes, these tests showed that the method reproduced observed climate statistics at annual, monthly, and daily time scales during both training and validation periods.

WGEN (Richardson and Wright 1984) generates these climate variables using serial-correlation (matrix A) and cross-correlation coefficients (matrix B):

$$X_i(j) = AX_{i-1}(j) + B\epsilon_i(j) \tag{1}$$

where $X_i(j)$ is a matrix including three climate variables (maximum temperature, minimum temperature and radiation) for day i. ϵ_i is a vector of independent random components. A and B are matrices that are calculated by

$$A = M_1 M_0^{-1} \tag{2}$$

$$BB^T = M_0 - M_1 M_0^{-1} M_1^T \tag{3}$$

where the elements of M_0 are the correlation coefficients on the same day and those of M_1 are the lag-1-day correlation coefficients. In the previous version of WGEN (Richardson and Wright 1984), only one set of elements for matrix A and B were given and applied across the entire continental USA. We used to apply same matrix values for A and B to other countries due to lacking of reported data on analytic solutions for matrix B in literature. Liu and Zuo (2012) first provided a derivation of the elements of matrix B to apply WGEN for downscaling with parameters derived specifically from their site. For downscaling WGEN parameters, historical climate data from 1960 to 2010 were sorted into 28 climate groups. WGEN parameters were then downscaled based on linear and non-linear relationships derived for the 28 climate groups from historical data and future GCM projections. The overall averaged confidence intervals between parameters and climate variables in our study were 0.08 and 0.11 (compared to a maximal value of 1.0) for observed mean and maximum values of climate variables, respectively, revealing a high confidence in extrapolating parameters for downscaling future climate. Downscaled daily sequences were finally evaluated to ensure that they were consistent with monthly GCM outputs in terms of monthly means or totals.

Two Representative Concentration Pathway scenarios (RCP4.5 and RCP 8.5) were considered in this study. RCP4.5 is a stabilization scenario where total radiative forcing is stabilized before 2100 by employment of a range of technologies and strategies for reducing greenhouse gas emissions. The RCP 8.5 is a high emissions scenario which is characterized by increasing greenhouse gas emissions. These two scenarios represent better and worse cases, respectively. Furthermore, these two scenarios have a larger collection of monthly temperature data in the CMIP5 archive than other RCPs, providing a larger sample size for more robust analysis.

2.4 Multi-model ensemble methods

Multi-model ensembles are commonly used in climate prediction to decrease the uncertainty of independent models. In addition to the arithmetic mean of model outputs, the IWM (independence weight mean) ensemble method was developed by Bishop and Abramowitz (2013) and was used to calculate multi-model mean values and heat stress indices. First, we calculated the four heat stress indices for each month (June to August) at each site during the period 1960–2010, producing 28 × 153 values for each site. The aim of IWM is to find the linear combination of an ensemble of model simulations that minimizes mean square difference (MSD) with respect to an observational dataset. That is to find

$$\sum_{j=1}^{J} \left(\mu_e^j - y^j\right)^2 \quad where \quad \mu_e^j = w^T x^j = \sum_{k=1}^{K} w_k x_k^j \tag{4}$$

is minimized with the additional constraint that $\sum_{k=1}^{K} w_k = 1$. The (1,…,*j*,…*J*) is time steps (in this study, *J* is 153 and *K* is 28) and this x_k^j is the *j*th time step of *k*th bias-corrected model. y^j is the *j*th time-step observation, w_k is the *k*th model coefficient (i.e., the weight in the linear combination).

$w^T = [w_1, w_2, \ldots w_K]$ and $(x^j)^T = \left[x_1^j, x_2^j, \ldots x_K^j\right]$. This requires minimizing the following function:

$$F(\boldsymbol{w}, \lambda) = \frac{1}{2}\left[\frac{1}{(J-1)} \sum_{j=1}^{J} \left(\mu_e^j - y^j\right)^2\right] - \lambda\left(\left(\sum_{k=1}^{K} w_k\right) - 1\right) \tag{5}$$

where λ is the Lagrange multiplier. The solution of Eq. 2 is

$$\mathbf{w} = \frac{\boldsymbol{A}^{-1}1}{1^T \boldsymbol{A}^{-1}1} \tag{6}$$

where 1^T=[1,1,…,1] and **A** is the *K*×*K* difference covariance matrix.

$$A = \left(\begin{bmatrix} c_{1,1} & \cdots & c_{1,K} \\ \vdots & \ddots & \vdots \\ c_{K,1} & \cdots & c_{K,K} \end{bmatrix}\right) \tag{7}$$

where $c_{i,j}$ is the covariance of the *i*th and *j*th bias-corrected model minus observed time serials.

After ensemble monthly mean values were obtained, we calculated heat stress indices in every year and for each site.

3 Results

3.1 Spatial variation of historical rice heat stress indices

There were strong spatial patterns in heat stress indices across the rice belt of southern China from 1960 to 2010 (Fig. 2). Heat stress was severe in the central and eastern areas of the

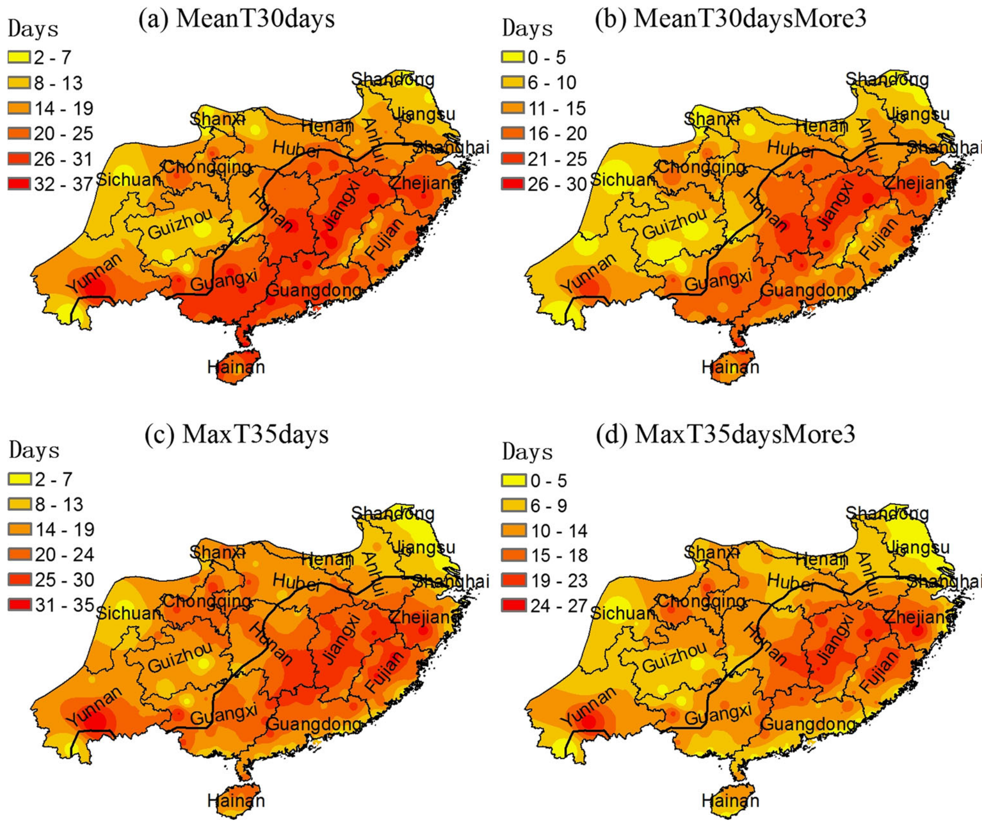

Fig. 2 The spatial distribution of average observed heat stress indices from 1960 to 2010 across rice planting region in southern China

double-harvest region, which includes portions of Hunan, Jiangxi, Zhejiang, and Fujian provinces. In the single season region, Chongqing province had the highest frequency of heat stress, whereas the Yungui Plateau (Yunnan and Guizhou province) province had the lowest frequency of heat stress due to its high altitude.

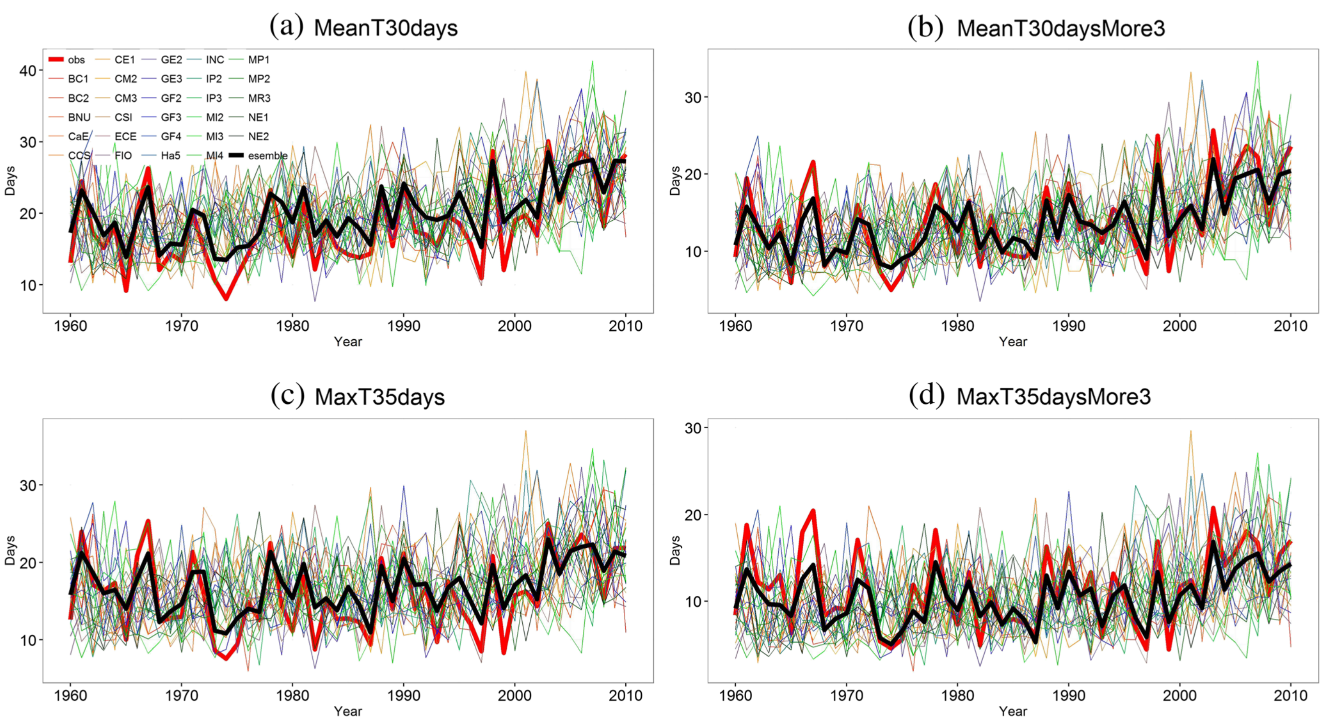

Fig. 3 Observed and simulated heat stress indices from individual models and the ensemble multi-model independence weight mean (IWM). Values are averaged across the rice-planting region of southern China

Table 3 Observed and simulated trends (days dacade^{-1} over 1960–2000) for the four heat stress indices. Italics signifies trends that are significant at the 5% level

GCMs	MeanT30days	MeanT30daysMore3	MaxT35days	MaxT35daysMore3
Observed	*1.69*	*1.52*	0.63	0.47
AM	*1.63*	*1.48*	*1.15*	*0.97*
IWM	*1.59*	*1.44*	0.73	*0.64*
BCC-CSM1.1	*2.13*	*1.98*	*1.52*	*1.29*
BCC-CSM1.1(m)	*1.40*	*1.29*	*0.98*	*0.80*
BNU-ESM	*1.76*	*1.65*	*1.06*	*0.97*
CanESM2	*1.75*	*1.59*	0.95	0.73
CCSM4	*2.65*	*2.46*	*1.98*	*1.70*
CESM1(BGC)	*2.16*	*1.96*	*1.75*	*1.41*
CMCC-CM	*1.71*	*1.68*	*1.04*	*0.96*
CMCC-CMS	*1.65*	*1.45*	*1.16*	*0.93*
CSIRO-Mk3.6.0	*1.30*	*1.18*	*0.85*	*0.65*
EC-EARTH	*1.54*	*1.38*	*0.99*	*0.82*
FIO-ESM	*1.72*	*1.55*	*1.31*	*1.10*
GISS-E2-H-CC	*1.81*	*1.68*	*1.32*	*1.16*
GISS-E2-R	*1.61*	*1.43*	*1.47*	*1.23*
GFDL-CM3	*1.44*	*1.28*	0.72	0.54
GFDL-ESM2G	*1.42*	*1.33*	0.78	0.68
GFDL-ESM2M	0.64	0.53	0.21	0.11
HadGEM2-AO	*1.94*	*1.82*	*1.27*	*1.07*
INM-CM4	*2.17*	*1.96*	*2.22*	*1.92*
IPSL-CM5A-MR	*1.75*	*1.57*	*1.43*	*1.17*
IPSL-CM5B-LR	*1.53*	*1.39*	*1.01*	*0.87*
MIROC5	0.04	0.08	−0.44	−0.36
MIROC-ESM	*1.47*	*1.34*	*1.04*	*0.88*
MIROC-ESM-CHEM	0.80	0.70	0.40	*0.33*
MPI-ESM-LR	*2.60*	*2.33*	*2.32*	*1.93*
MPI-ESM-MR	*2.93*	*2.67*	*2.53*	*2.20*
MRI-CGCM3	0.42	0.36	−0.10	−0.11
NorESM1-M	*2.13*	*1.93*	*1.60*	*1.37*
NorESM1-ME	*1.11*	*0.97*	*1.00*	*1.29*

Of the four heat stress indices, *meanT30days* resulted in the largest distribution of heat stress between 1960 and 2010. *MeanT30days* hot spots in Hunan, Jiangxi, Zhejiang, Guangxi, and Guangdong typically persisted for 26 to 37 days (Fig. 2). By contrast, the average value of *meanT30daysMore3* was reduced to 21–25 days in three provinces: southeast Hunan province, most of of Jiangxi province and central Zhejiang, although this was still double or triple the heat stress experienced in other parts of study region. Similarly, values of *maxT35days* and *maxT35daysMore3* were high in the regions where *meanT30days* and *meanT30daysMore3* were high, although the average values of *maxT35days* and *maxT35daysMore3* were smaller (up to 25–30 days and 19–23 days, respectively).

3.2 Comparison between observed and downscaled heat stress indices

Figure 3 shows the observed and downscaled values of each heat stress index from 1960 to 2010 across the rice belt in southern China. Table 3 shows the trends and their significance in observed and simulated heat stress indices. There were significant, increasing trends for observed and modeled *MeanT30days* and *MeanT30daysMore3* except in four GCMs (GFDL-ESM2M, MIROC5, MIROC-ESM-CHE, and MRI-CGCM3). AM produced similar trends to observations in *MeanT30days* and *MeanT30daysMore3* (Table 3). The observed indices *MaxT35days* and *MaxT35daysMore3* showed no significant trend, whereas

Table 4 Root-mean-square error (RMSE) between observations and multi-model arithmetic mean (AM), independence weighted mean (IWM), or individual GCMs during 1960–2000

GCMs	MeanT30days	MeanT30daysMore3	MaxT35days	MaxT35daysMore3
AM	9.57	8.92	8.93	8.12
IWM	7.08	6.41	6.59	5.88
BCC-CSM1.1	11.53	11.16	10.90	10.16
BCC-CSM1.1(m)	11.98	11.49	11.22	10.44
BNU-ESM	11.33	10.93	10.74	9.97
CanESM2	11.91	11.46	11.37	10.67
CCSM4	13.10	12.50	12.64	11.72
CESM1(BGC)	13.01	12.43	12.19	11.29
CMCC-CM	11.54	11.02	10.97	10.15
CMCC-CMS	12.15	11.72	11.54	10.68
CSIRO-Mk3.6.0	12.27	11.80	11.84	10.91
EC-EARTH	11.99	11.49	11.41	10.54
FIO-ESM	12.01	11.54	11.51	10.61
GISS-E2-H-CC	12.74	12.21	11.84	11.02
GISS-E2-R	11.86	11.40	11.27	10.39
GFDL-CM3	11.43	11.11	11.09	10.36
GFDL-ESM2G	11.98	11.51	11.55	10.70
GFDL-ESM2M	11.89	11.59	11.35	10.65
HadGEM2-AO	11.42	11.00	10.96	10.15
INM-CM4	11.53	11.17	11.84	11.04
IPSL-CM5A-MR	11.49	11.09	11.94	11.02
IPSL-CM5B-LR	11.60	11.10	11.67	10.73
MIROC5	12.06	11.66	11.42	10.60
MIROC-ESM	12.37	12.01	11.60	10.86
MIROC-ESM-CHEM	11.74	11.31	11.19	10.38
MPI-ESM-LR	11.96	11.44	11.41	10.47
MPI-ESM-MR	12.66	12.12	11.94	10.99
MRI-CGCM3	11.35	11.08	10.90	10.26
NorESM1-M	11.34	10.99	11.23	10.49
NorESM1-ME	11.42	11.13	10.94	10.30

21 of the GCMs had significant trends but with two models displaying a negative trend (MIROC5 and MRI-CGCM3; Table 3).

Inter-annual variability was large in both observed and simulated heat stress indices (Fig. 3). The variability of IWM simulations from 28 GCMs was less than that of the individual models. Additionally, the IWM ensemble results had good consensus with observations (Fig. 3). Table 4 shows the root-mean-square error (RMSE) values which were calculated between the multi-model arithmetic mean (AM), independence weighted mean (IWM), each GCM, and observed values for the four heat stress indices during 1960–2000. All GCMs had larger RMSE than the ensemble values (AM or IWM), and the RMSE for IWM was smallest (Table 4).

3.3 Multi-model ensemble projections of heat stress in the twenty-first century

Spatial differences in multi-model ensemble (IWM) heat stress indices between 1960–2010 and 2061–2100 for RCP8.5 (i.e., increasing emissions scenario) are shown as Fig. 4. Heat stress will increase across the rice belt of southern China between 1960–2010 and 2061–2100, regardless of the heat stress index used. Not only will heat stress increase across the region, there are no locations where heat stress is expected to decline (Fig. 4). The most spatially consistent increase of *MeanT30days* and *MeanT30daysMore3* was in the middle and lower reaches of Yangtze River, including Chongqing, Hunan, Hubei, and Jiangxi provinces. The annual number of heat stress days showed increases across this region by 47–67 and 43–64 days in the *MeanT30days* and

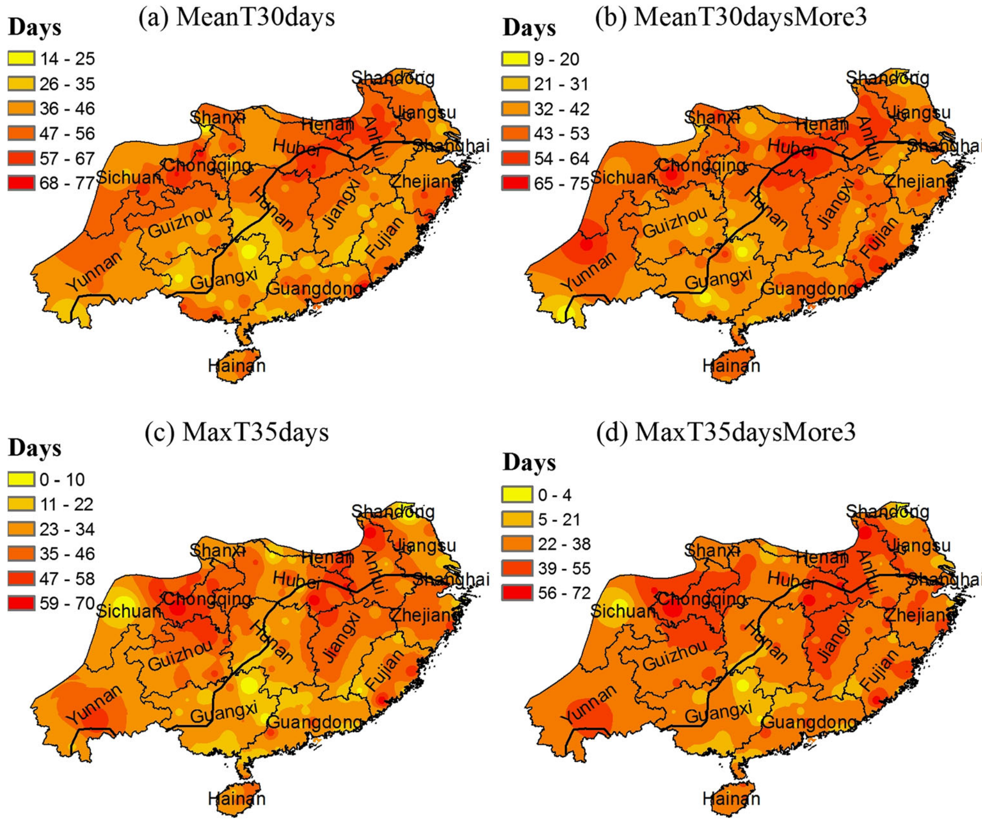

Fig. 4 Changes in multi-model ensemble (IWM) simulated heat stress indices during the period 2061–2100 compared to 1960–2000 under RCP 8.5

MeanT30daysMore3 indices, respectively. Using either the *MeanT30days* or *MeanT30daysMore3* index, heat stress will consistently increase over the twenty-first century under both emissions scenarios (RCP 4.5 with stable emissions and RCP8.5) (Fig. 5a–b). In comparison to the reference period (1960–2010), *MeanT30days* increased dramatically (by ca. 142.5% under RCP 4.5 and 223% under RCP8.5). By the end of twenty-first century, *MeanT30daysMore3* showed increases of approximately 185.2 and 319% under emissions scenarios RCP4.5 and RCP8.5, respectively.

The maximum-temperature indices, *MaxT35days* and *MaxT35daysMore3*, also increased across the rice belt in 2061–2100 by 0–70 and 0–72 days, respectively (Fig. 4c–d). Increases were largest in Chongqing, east of Hubei, and Jiangxi provinces with a range of 47–70 days for *MaxT35days* and of 39–72 days for *MaxT35daysMore3*. By the end of twenty-first century, *MaxT35days* will have increased dramatically by about 118.2% for RCP4.5 and 208.2% for RCP8.5, and *MaxT35daysMore3* will have increased by about 167.5 and 296.5% for RCP4.5 and RCP8.5, respectively (Fig. 5c–d).

4 Discussion

As hypothesized, heat stress in the Chinese rice belt has been shown to increase during the historical period (1960–2010; Table 3) as well as in climate projections through the twenty-first century (Fig. 5). Spatially, heat stress was distributed across the southern and eastern regions which produce two crops per season (the double season region), whereas the largest projected increases in heat stress were predicted for these provinces. The historical increase was consistent with the results of Zhang et al. (2014) and Shi et al. (2015a), who used alternative heat stress indices. For example, the cumulative exposure to extreme temperatures (GDD) has increased by 2.25 °C in single rice in the Yangtze River basin, and by 4.42 °C in the double-season rice region of southern China (Zhang et al. 2014). Similarly, the accumulated days of heat stress (ADHS) index showed an increasing trend from 1981 to 2010 of 1.2 days per decade in the eastern double-season rice region (Shi et al. 2015a), which was smaller than our results (1.52–1.69 days per decade in Table 3). The smaller rates in the study by Shi et al. (2015a) are due to compensation by rice phenology, which was not considered in our study.

The ensemble heat stress indices from downscaled GCM data were representative of the pattern of observed heat stress over the whole region as indicated by the high temporal consistency between simulated and observed trends (Fig. 3) and small RMSEs (Table 4). However, the trends produced by some individual GCMs was opposite to observed values

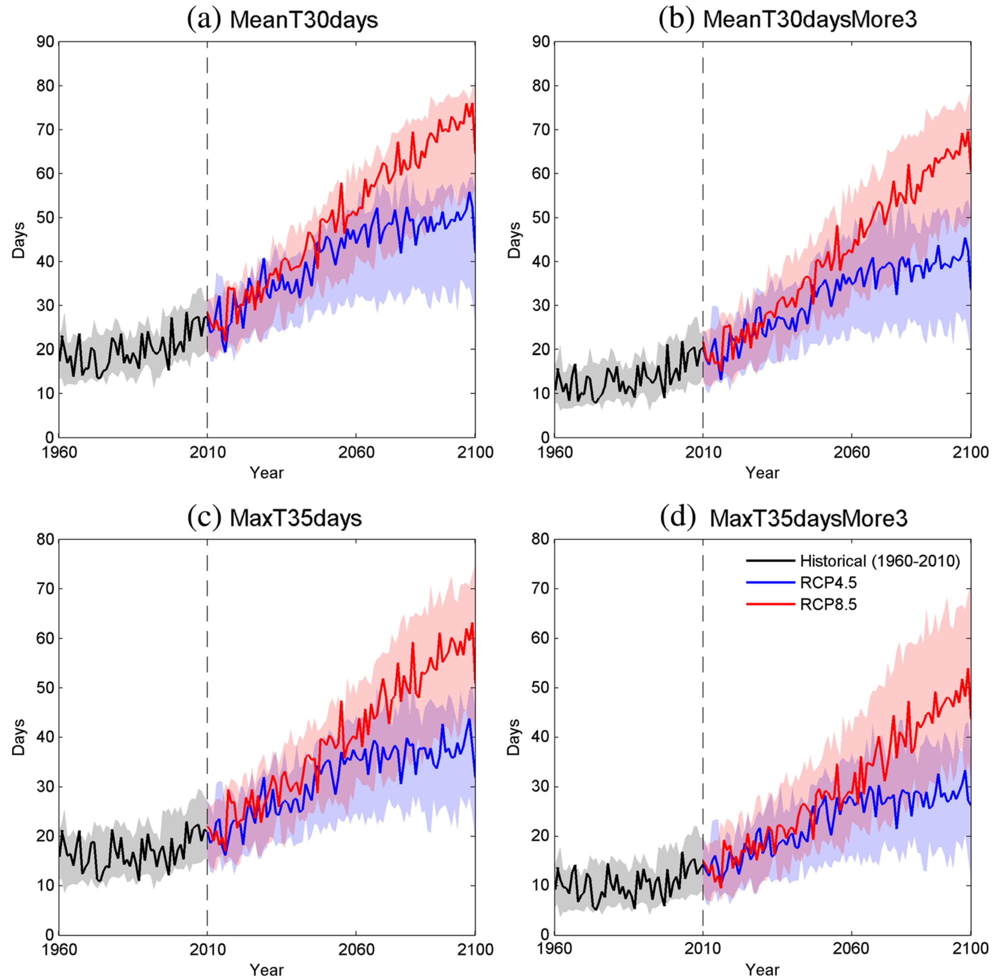

Fig. 5 Time series of multi-model ensemble simulated heat stress indices under RCP 4.5 and RCP 8.5 averaged across the rice planting region in southern China

(e.g., *MaxT35daysMore3* from MIROC5; Table 3), although these reverse trends were not significantly different from zero. Individual differences among GCMs notwithstanding, the close consistency between ensemble results and observations are expected due to the empirical relationships relied upon by statistical downscaling methods (Liu and Zuo 2012). Furthermore, extreme heat stress may not be well represented in individual GCMs, while other models might overestimate extremes, thus errors compensated to produce better correspondence between observed data and ensemble results. This lends confidence to the ensemble results for representing future scenarios.

Our results also showed that there was a significant increase in heat stress indices over the whole rice belt both in RCP 4.5 (emissions leveled off) and RCP 8.5 (increasing emissions) scenarios. The results were similar to previous results (Jiang et al. 2012; Xu et al. 2009; Zhou et al. 2014) which presented the projection of extreme temperature change over the whole China using ensemble results of multi-models. Jiang et al. (2012) evaluated heat wave duration index (HWDI) based on observed and GCM simulations in CMIP3, finding HWDI would increase by 35 to 90 days in various scenarios by the end of 21st. Zhou et al. (2014) illustrated that the median of TX90p (percentage of days when the daily maximum temperature is above the 90th percentile) will increase in southern China by the end of twenty-first century from 10% in the base period to 36% under RCP4.5 and 59% under RCP8.5. Our study offers alternative heat stress indices which produce consistent trends to those of Jiang et al. (2012) and Zhou et al. (2014), indicating extreme warming in the future will be more serious. In addition, this study provided higher fine-scale resolution of future heat stress over the rice belt using IWM method than previous studies which focused on grid scales which are too coarse for accurate estimates of relevance for rice production.

The high risk of exposure to heat stress for rice in a warmer future world emphasizes the importance of promoting specific adaptations or mitigation strategies, especially to the north of the two-season line where heat was lower in the historical period but increased more in future scenarios. The flowering and grain-filling stages are most sensitive in rice to damage by heat stress. Even short episodes (less than 1 h) of heat stress during flowering can cause pollination failure, which reduces seed number and grain yield (Jagadish et al. 2007; Shi et al.

2015a). In addition, photosynthetic assimilation is reduced during grain filling, and the grain-filling period can be shortened due to heat stress. Damage to rice crops can be partially minimized by adjustment of the sowing date to avoid heat stress during key reproductive stages (Wassmann et al. 2009). Some modeling results (Krishnan et al. 2007; Wang et al. 2014a) indicated that advancing the sowing date can avoid heat stress and improve rice yield.

Increases in heat stress will exceed 50 days per year in some locations, which could reduce the efficacy of shifting the timing of the growing season and have disastrous effects on rice yield in the future. Thus more effort in breeding technology is crucial. Heat-tolerant cultivars should be planted widely throughout the region. Wang et al. (2014a) showed using the CERES model with two emissions scenarios that selecting very heat-resistant cultivars and altering the planting date can increase rice yields in Jiangsu province. From our results, heat stress risk in the middle and lower reaches of Yangtze River is highest in the future, where rice planting is extensive. Furthermore, risk of disaster increases due to the interaction of other extreme events like floods, which occur at high frequency in these rice-producing provinces of China.

The uncertainty in this study are from following aspects: (1) differences in the greenhouse gas emissions pathway (RCP scenario uncertainty), (2) differences due to the choice of GCM (GCM uncertainty), (3) differences due to the inter-annual variability of the climate system, and (4) differences due to statistical downscaling methods (e.g., failure to capture future extreme events, such as heavy daily precipitation or heatwaves). Uncertainty due to choice of RCP scenario or GCM was minimized by selecting a diversity of GCMs (28 in CMIP5) and applying two emissions scenarios (RCP4.5 and RCP8.5). Uncertainty due to our inability to model increasing inter-annual variability and extreme events in a future climate (Frank et al. 2015) is unavoidable. The 2003 heatwave in Europe is a key example of a temperature extreme which was statistically very unlikely (Schär et al. 2004), but the probability of predicting such a heatwave is improved in RCP8.5 relative to RCP4.5 (Russo et al. 2015). We found a similarly higher likelihood of heatwaves in RCP8.5 than in RCP4.5 (Fig. 5), suggesting that statistical uncertainty (i.e., due to variability and extremes) was minimized in the results from RCP8.5. No approach is complete without uncertainty, but sources of uncertainty in this study were minimized in as much as is practical at the current time.

There are some limitations in this study. Firstly, phenology of rice and timing of heat stress in the future is not considered when calculating the heat stress indices, thus overestimating the effect of heat stress in the future. Moreover, rice yield was not predicted in future scenarios in our study. Prediction of phenology, timing, and yield into the future is dependent upon the specific management adaptations that are applied in response to the way climate change unfolds. This requires further research into specific management scenarios.

5 Conclusions

Four heat stress indices were calculated using downscaled ensemble data from 28 CMIP5 GCMs. Ensemble model output using the independence weighted mean (IWM) method replicated the historical trend of heat stress indices over the period of 1960–2010. Additionally, RMSE between observed heat stress indices and ensemble results (6.5 days) was smaller than for individual GCM simulations (11.4 days), which indicated that the ensemble heat stress indices based on multiple models can reduce the uncertainty due to shortages in any single model. We found that there will be more heat stress events (by 118–319%) over the rice belt in southern China by the end of twenty-first century, especially in the middle and lower reaches of Yangtze River where heat stress has been historically small. These findings indicate that rice in southern China will have higher frequency of exposure to heat stress in the future (by up to 72 days of temperatures above the physiological tolerance of 30 °C). Thus, selection for heat-tolerant cultivars and adjustment of planting dates to avoid heat stress periods should be adopted to adapt to the effects of climate change on rice production in southern China.

Acknowledgements This study was supported by the Talent Project Plan (Thousand Talents Program) in Northwest A&F University, Special Fund for Public Welfare Industry (Meteorology, No.GYHY201506001), and National Natural Science Foundation of China (No. 41371119).

References

Anwar MR, Liu DL, Farquharson R et al (2015) Climate change impacts on phenology and yields of five broadacre crops at four climatologically distinct locations in Australia. Agric Syst 132:133–144

Bishop CH, Abramowitz G (2012) Climate model dependence and the replicate Earth paradigm. Clim Dyn 41:885–900

Frank D, Reichstein M, Bahn M, Thonicke K, Frank D, Mahecha MD, Smith P, van der Velde M, Vicca S, Babst F, Beer C, Buchmann N, Canadell JG, Ciais P, Cramer W, Ibrom A, Miglietta F, Poulter B, Rammig A, Seneviratne SI, Walz A, Wattenbach M, Zavala MA, Zscheischler J (2015) Effects of climate extremes on the terrestrial carbon cycle: concepts, processes and potential future impacts. Glob Chang Biol 21(8):2861–2880

Huang J, Zhang F, Xue Y, Lin J (2016) Recent changes of rice heat stress in Jiangxi province, southeast China Int J Biometeorol:1–11 doi: https://doi.org/10.1007/s00484-016-1239-3

IPCC (2013) Climate change 2013: the physical science basis. Contribution of working group I to the fifth assessment report of the intergovernmental panel on climate change, [Stocker, T. F., D. Qin, G.-K. Plattner, M. Tignor, S. K. Allen, J. Boschung, A. Nauels, Y. Xia, V. Bex and P. M. Midgley (eds.)]. Cambridge, United Kingdom and New York, NY, USA in press

Jagadish SV, Craufurd PQ, Wheeler TR (2007) High temperature stress and spikelet fertility in rice (Oryza sativa L.) J Exp Bot 58:1627

Jagadish SVK, Murty MVR, Quick WP (2014) Rice responses to rising temperatures—challenges, perspectives and future directions. Plant Cell Environ 38:1686–1698

Jiang Z, Song J, Li L, Chen W, Wang Z, Wang J (2012) Extreme climate events in China: IPCC-AR4 model evaluation and projection. Clim Chang 110:385–401

Knutti R, Sedlacek J (2013) Robustness and uncertainties in the new CMIP5 climate model projections. Nat Clim Change 3:369–373

Krishnan P, Swain DK, Chandra Bhaskar B, Nayak SK, Dash RN (2007) Impact of elevated CO2 and temperature on rice yield and methods of adaptation as evaluated by crop simulation studies. Agric, Ecosyst Environ 122:233–242. doi:https://doi.org/10.1016/j.Agee.2007.01.019

Liu DL, Zuo H (2012) Statistical downscaling of daily climate variables for climate change impact assessment over New South Wales. Aust Clim Chang 115:629–666

Peng SB et al (2004) Rice yields decline with higher night temperature from global warming. Proc of the Natl Acad of Sci of the U S A 101: 9971–9975. doi:https://doi.org/10.1073/pnas.0403720101

Piao S et al (2010) The impacts of climate change on water resources and agriculture in China. Nature 467:43–51

Richardson CW, Wright DA (1984) WGEN: a model for generating daily weather variables. U. S. Department of Agriculture, Agricultural Research Service

Russo S, Sillmann J, Fischer EM (2015) Top ten European heatwaves since 1950 and their occurrence in the coming decades. Environ Res Lett 10(12):124003

Sánchez B, Rasmussen A, Porter JR (2014) Temperatures and the growth and development of maize and rice: a review. Glob Chang Biol 20: 408–417

Schär C, Vidale PL, Lüthi D, Frei C, Häberli C, Liniger MA, Appenzeller C (2004) The role of increasing temperature variability in European summer heatwaves. Nature 427(6972):332–336

Shen X, Liu B, Lu X, Fan G (2016) Spatial and temporal changes in daily temperature extremes in China during 1960–2011 Theor Appl Climatol:1–11 doi:https://doi.org/10.1007/s00704-016-1934-3

>Shi P, Tang L, Lin C, Liu L, Wang H, Cao W, Zhu Y (2015a) Modeling the effects of post-anthesis heat stress on rice phenology. Field Crop Res 177:26–36

Shi P, Liang T, Wang L, Sun T, Liu L, Cao W, Zhu Y (2015b) Post-heading heat stress in rice of South China during 1981-2010 PLoS One 10

Shuai Z, Tao F, Zhao Z (2014) Rice reproductive growth duration increased despite of negative impacts of climate warming across China during 1981–2009. Eur J Agron 54:70–83

Sillmann J, Roeckner E (2008) Indices for extreme events in projections of anthropogenic climate change. Clim Chang 86:83–104

Sun W, Huang Y (2011) Global warming over the period 1961–2008 did not increase high-temperature stress but did reduce low-temperature stress in irrigated rice across China. Agric For Meteorol 151:1193–1201. doi:https://doi.org/10.1016/j.Agrformet.2011.04.009

Sun Y et al (2014) Rapid increase in the risk of extreme summer heat in Eastern China. Nat Clim Chang 4:1082–1085

Tao F, Zhang Z (2013) Climate change, high-temperature stress, rice productivity, and water use in eastern china: a new superensemble-based probabilistic projection. J Appl Meteorol Climatol 52:531–551

Tao F et al (2014) Responses of wheat growth and yield to climate change in different climate zones of China, 1981–2009. Agric For Meteorol 189–190:91–104. doi:https://doi.org/10.1016/j.Agrformet.2014.01.013

Tebaldi C, Knutti R (2007) The use of the multi-model ensemble in probabilistic climate projections Philosophical Transactions of the Royal Society A: Mathematical. Phys Eng Sci 365:2053–2075. doi:https://doi.org/10.1098/rsta.2007.2076

Tebaldi C, Smith RL, Nychka D, Mearns LO (2005) Quantifying uncertainty in projections of regional climate change: a bayesian approach to the analysis of multimodel ensembles. J Clim 18:1524–1540. doi:https://doi.org/10.1175/JCLI3363.1

Vaittinada Ayar P, Vrac M, Bastin S, Carreau J, Déqué M, Gallardo C (2016) Intercomparison of statistical and dynamical downscaling models under the EURO- and MED-CORDEX initiative framework: present climate evaluations. Clim Dyn 46:1301–1329. doi:https://doi.org/10.1007/s00382-015-2647-5

Wang B, Liu DL, Macadam I, Alexander LV, Abramowitz G, Yu Q (2016) Multi-model ensemble projections of future extreme temperature change using a statistical downscaling method in south eastern Australia. Clim Chang 138:1–14

Wang L, Ren J, Li Q (2014a) Simulation of the heat injury on rice production in Jiangsu Province under the climate change scenarios II: adaptability analysis of the rice to heat injury from booting to heading stage. Chin J Agrometeorol 35:206–213

Wang P, Zhang Z, Song X, Chen Y, Wei X, Shi P, Tao F (2014b) Temperature variations and rice yields in China: historical contributions and future trends. Clim Chang 124:777–789

Wassmann R et al. (2009) Chapter 3 regional vulnerability of climate change impacts on Asian rice production and scope for adaptation. In: Advances in agronomy, vol volume 102. Academic Press, pp 91–133. Doi:https://doi.org/10.1016/S0065-2113(09)01003-7

Xu Y, Xu C, Gao X, Luo Y (2009) Projected changes in temperature and precipitation extremes over the Yangtze River Basin of China in the 21st century. Quat Int 208:44–52

Yang YM, Liu DL, Anwar MR, Zuo HP, Yang YH (2014) Impact of future climate change on wheat production in relation to plant-available water capacity in a semiaridenvironment. Theor Appl Climatol 115(3): 391–410

Yao F, Xu Y, Lin E, Yokozawa M, Zhang J (2007) Assessing the impacts of climate change on rice yields in the main rice areas of China. Clim Chang 80:395–409. doi:https://doi.org/10.1007/s10584-006-9122-6

Zhang S, Tao F, Zhang Z (2016) Changes in extreme temperatures and their impacts on rice yields in southern China from 1981 to 2009. Field Crop Res 189:43–50

Zhang T, Huang Y, Yang X (2013) Climate warming over the past three decades has shortened rice growth duration in China and cultivar shifts have further accelerated the process for late rice. Glob Chang Biol 19:563–570

Zhang Z, Wang P, Chen Y, Song X, Wei X, Shi P (2014) Global warming over 1960–2009 did increase heat stress and reduce cold stress in the major rice-planting areas across China. Eur J Agron 59:49–56

Zhou B, Wen QH, Xu Y, Song L, Zhang X (2014) Projected changes in temperature and precipitation extremes in China by the CMIP5 multimodel ensembles. J Clim 27:6591–6611